



3 4456 0387874 8

ORNL/TM-12795

**ornl**

**OAK RIDGE  
NATIONAL  
LABORATORY**

**MARTIN MARIETTA**

**Measurements and Modeling of  
Impurity Source Distributions from  
the Tore Supra Outboard Pump  
Limiter**

C. C. Klepper

J. T. Hogan  
S. J. Tobin  
R. C. Isler

D. Guilhem  
W. R. Hess  
P. Monier-Garbet

OAK RIDGE NATIONAL LABORATORY

CENTRAL RESEARCH LIBRARY

CIRCULATION SECTION

4500N ROOM 175

**LIBRARY LOAN COPY**

DO NOT TRANSFER TO ANOTHER PERSON

If you wish someone else to see this  
report, send in name with report and  
the library will arrange a loan.

UCN-7969 (3 9-77)

MANAGED BY  
MARTIN MARIETTA ENERGY SYSTEMS, INC.  
FOR THE UNITED STATES  
DEPARTMENT OF ENERGY

This report has been reproduced directly from the best available copy.

Available to DOE and DOE contractors from the Office of Scientific and Technical Information, P.O. Box 62, Oak Ridge, TN 37831; prices available from (615) 576-8401, FTS 626-8401.

Available to the public from the National Technical Information Service, U.S. Department of Commerce, 5285 Port Royal Rd., Springfield, VA 22161.

This report was prepared as an account of work sponsored by an agency of the United States Government. Neither the United States Government nor any agency thereof, nor any of their employees, makes any warranty, express or implied, or assumes any legal liability or responsibility for the accuracy, completeness, or usefulness of any information, apparatus, product, or process disclosed, or represents that its use would not infringe privately owned rights. Reference herein to any specific commercial product, process, or service by trade name, trademark, manufacturer, or otherwise, does not necessarily constitute or imply its endorsement, recommendation, or favoring by the United States Government or any agency thereof. The views and opinions of authors expressed herein do not necessarily state or reflect those of the United States Government or any agency thereof.

Fusion Energy Division

**Measurements and Modeling of Impurity Source Distributions from the  
Tore Supra Outboard Pump Limiter\***

C. C. Klepper

J. T. Hogan  
S. J. Tobin<sup>†</sup>  
R. C. Isler

D. Guilhem<sup>‡</sup>  
W. R. Hess<sup>‡</sup>  
P. Monier-Garbet<sup>‡</sup>

---

\*An annotated version of the paper presented at the 11th International Conference on Plasma Surface Interactions in Controlled Fusion Devices, May 23–27, 1994, Mito, Japan.

<sup>†</sup>Oak Ridge Association of Universities

<sup>‡</sup>Association EURATOM-CEA

Date Published: August 1994

Prepared for the  
Office of Fusion Energy  
Budget Activity No. AT 10-10-14-Z

Prepared by  
OAK RIDGE NATIONAL LABORATORY  
Oak Ridge, Tennessee 37831  
managed by  
MARTIN MARIETTA ENERGY SYSTEMS, INC.  
for the  
U.S. DEPARTMENT OF ENERGY  
under contract DE-AC05-84OR21400





## CONTENTS

	<b>Page</b>
ABSTRACT .....	1
INTRODUCTION .....	1
Model Description .....	3
Experimental Setup .....	6
Experimental Results .....	7
DISCUSSION AND CONCLUSIONS .....	8
ACKNOWLEDGMENTS .....	9
REFERENCES .....	9



# MEASUREMENTS AND MODELING OF IMPURITY SOURCE DISTRIBUTIONS FROM THE TORE SUPRA OUTBOARD PUMP LIMITER\*

C. C. Klepper, J. T. Hogan, S. J. Tobin,† R. C. Isler  
Fusion Energy Division, Oak Ridge National Laboratory

D. Guilhem, W. R. Hess, P. Monier-Garbet  
Assoc. EURATOM- CEA, DRFC/SPPF, Centre d'Etudes de Cadarache

## ABSTRACT

An experiment has been carried out to study impurity generation processes on an inertial limiter on Tore Supra. It is part of a plan to assemble a more detailed integrated picture of impurity generation at the inner wall, the outboard and vertical pump limiters, and the heating and current drive antennas. A system has been implemented to permit quantitative measurement of impurity sources from the outboard limiter in Tore Supra. Data are presented for a representative case in which the limiter is isolated as much as possible from connection with other Tore Supra plasma-facing components. The data are compared with results from the Monte-Carlo SOL impurity transport code BBQ, in an attempt to identify the mechanism for impurity release. Evidence of chemical sputtering as an important impurity source is seen.

## INTRODUCTION

The problem of impurity generation presents a fundamental limit to long pulse, steady-state operation. To characterize the impurity source accurately in a tokamak experiment, it is necessary to understand the interrelationship of sources from all the plasma-facing components (PFCs). In Tore Supra, these include the inner wall, the outboard and vertical pump limiters, as well as the heating and current drive antennas. As is well known, however, impurity transport at the plasma edge is not well understood and is hard to measure experimentally. Measurement and interpretation of edge impurity generation and transport are complicated because the sources are very localized and the atomic and molecular processes are complex. The highly localized nature of the sources, and of the associated optical emission, implies that good spectroscopic viewing access and high spatial resolution are required. Since the spatial distributions of charged impurities are the typical observables, interpretation in terms of generation processes requires

---

\*Research sponsored in part by the U.S. Department of Energy (U.S. DOE), and carried out under contract DE-AC05-84OR21400 with Martin Marietta Energy Systems, Inc., and under the international collaboration agreement between the U.S. DOE and the Association EURATOM-CEA.

†Supported by a fellowship from the Oak Ridge Association of Universities.

the use of codes to translate the predicted distribution of impurity densities from a given source into an observed distribution of emission. It also requires that the codes used in the interpretation include the specific geometry of PFCs in great detail.

This paper describes a study conducted on Tore Supra in which small plasmas were created to isolate the outboard limiter as the most important PFC. Complementing previous studies of impurity generation at the Tore Supra inner wall [1], [2] and the neutralizer plate of a previously installed outboard pump limiter [2], [3], this study allows an examination of the characteristics of impurity generation at the face of the outboard limiter in isolation from other interactions. Since there is no direct view of this limiter from an external port in the machine, the design of a special endoscopic imaging system was required, and this is described below.

For modeling and interpretation of the data the impurities code BBQ is used. This code incorporates a 3-D Monte-Carlo description of both neutral and charged impurity transport. The “physical” model in the code is patterned after that in the LIM code (P. Stangeby et al. [4]). As is well known, the value of such codes is determined by the level of detail of geometry which is included, and the detailed, “as-built”, geometry of Tore Supra is incorporated in BBQ. For the impurity generation processes, such as physical and chemical sputtering, the recommended values of Eckstein et al. [5] are employed. BBQ calculates the evolution of  $\text{CH}_4$  breakup products (chemically produced impurities) using the data base of Erhardt and Langer [6]. The  $\text{CH}_4$  breakup model in BBQ was compared with low density experiments conducted in PISCES [7]. The code calculates spatial distributions of  $\text{C}^0 \rightarrow \text{C}^{+6}$  (and of  $\text{CH}_4 \rightarrow \text{CH}$ ) arising from impurity generation.

This experiment was carried out with an inertially cooled, nonpumping outboard limiter (Phase I). The Tore Supra semi-actively cooled (Phase II) pump limiter used in previous experiments had been removed to repair damage incurred in a previous experiment. The front face of the Phase I inertially cooled limiter is shaped identically to that of the new, actively cooled Phase III pump limiter, which is presently installed on Tore Supra [8]. The Phase I limiter is a monoblock of isotropic graphite and is not cooled. As a result, the plasma contact with the outboard limiter module was limited to about 4 s, and time-dependent effects were anticipated because of the increasing temperature of the limiter.

The shape of the outboard limiter was designed from optimization studies that accounted for the detailed magnetic flux geometry, including ripple effects, to optimize the heat removal capability, while keeping the heat flux to the leading edge within a manageable range [9], [10], [11]. Figure 1 shows the predicted toroidal heat flux distribution for the design case of  $R = 2.38$  m,  $a = 0.75$  m on the limiter [11]. Note in Fig. 1 that maximum limiter temperatures are expected near the “crown” of the front face (at 0.10 to 0.15 m toroidally from the tangency point) and at the tip of the leading edge.

## Model Description

### General scheme

The code sequence begins with a calculation of physical sputtering arising from  $D^+ - C$  interactions, so that the spatial and velocity distribution of neutral ( $C^0$ ) atoms entering the SOL plasma is computed. The  $D^+$  flux is calculated from an exponential-sine model, or with an assumed flux-amplified particle flux distribution. The BBQ code then calculates the further evolution of these atoms as they are ionized, transported parallel and perpendicular to field lines in the SOL, are further ionized or recombine or undergo charge exchange with  $D^0$  to lower charge states, and finally either strike a PFC, or enter into the well-confined core plasma region. The spatial and energy distribution of  $C^{n+}$  ions which terminate on other PFCs is recorded, including the energy gain by sheath acceleration by the  $n$ -tuply-charged ions. This information is then used for a next stage, where the transport of the impurities produced by this self-sputtering is tracked. The process is continued as long as required. An estimate of the sum of the geometric series for the total sputtering yield,  $Y_{\text{eff}} = Y_{\text{DC}}/(1 - \eta Y_{\text{CC}})$  ( $= Y_{\text{DC}} + \eta Y_{\text{CC}} - \dots$ ) can be made, where  $Y_{\text{DC}}$  is the  $D \rightarrow C$  sputter yield,  $Y_{\text{CC}}$  is the C self-sputter yield and  $\eta$  is the self-sputter probability. The distributions for the ions reaching the confinement zone are saved as input to radial impurity transport (Mattioli code) calculations.

### D $\rightarrow$ C impurity generation stage

The particle [heat] fluxes are assumed to obey an exponential relation, with a characteristic scrape-off layer length  $\lambda_{\Gamma}$  [ $\lambda_q$ ], with  $\Gamma_{\parallel}(\rho)$ ,  $\Gamma_{\perp}(\rho)$ ,  $q_{\parallel}(\rho)$ , and  $q_{\perp}(\rho)$  defined as

$$\Gamma(\rho) = \mathbf{b} \Gamma_{\parallel}(a) e^{-(r-a)/\lambda_{\Gamma}} + \mathbf{n} \Gamma_{\perp}(a) e^{-(\rho-a)/\lambda_{\Gamma}} , \quad (1)$$

and, for the heat flux,

$$q(\rho) = \mathbf{b} q_{\parallel}(a) e^{-(r-a)/\lambda_q} + \mathbf{n} q_{\perp}(a) e^{-(\rho-a)/\lambda_q} , \quad (2)$$

for  $\rho \geq a$  where  $\mathbf{n}(\equiv \nabla\psi/|\nabla\psi|)$ ,  $\psi$ : poloidal flux) is the unit vector normal to the poloidal flux surface and  $\mathbf{b}(\equiv \mathbf{B}/|\mathbf{B}|)$  is the unit vector parallel to the magnetic field. The quantities  $\Gamma_{\parallel}(a)[q_{\parallel}(a)]$  and  $\Gamma_{\perp}(a)[q_{\perp}(a)]$  are the particle [heat] fluxes at the outermost plasma surface tangent to the PFC at the equator ( $\rho = a$ ). We assume a value for the ratio of perpendicular and parallel fluxes as a free parameter (since it cannot be directly measured).

Thus, we define

$$F_{\parallel,\perp} \equiv \Gamma_{\parallel}(a)/\Gamma_{\perp}(a) , \quad (3)$$

and

$$Q_{\parallel,\perp} \equiv q_{\parallel}(a)/q_{\perp}(a) . \quad (4)$$

The flux of  $D^+$  and heat to the PFCs is proportional to the components of the parallel and perpendicular fluxes normal to these surfaces. The value of the fluxes to the surface at radius  $\rho$  are thus, for the particle flux normal to the surface:

$$\Phi_{\perp}(r) = \Gamma_{\parallel}(\rho) \sin(\phi) + \Gamma_{\perp}(\rho) \cos(\phi) , \quad (5)$$

and the heat flux normal to the surface is

$$H_{\perp}(\rho) = q_{\parallel}(\rho) \sin(\phi) + q_{\perp}(\rho) \cos(\phi) . \quad (6)$$

Here  $\phi$  is the local angle of incidence between the PFC surface and the plasma flux surface.

The effective sputtering yield for  $D \rightarrow C$  is taken from the Roth et al. [7] semi-empirical model. The enhancement in this sputtering yield for oblique angles of incidence is estimated with the model of Yamamura et al., which is also discussed in [7]. In the present calculations we limit the maximum increase over the normal-incidence yield to a factor 2. The sputtering yield is calculated using local plasma parameters at the tile surface, assuming an exponential radial dependence of plasma parameters in the SOL as described in Eqs. (1) and (2). The local sheath potential is assumed to be  $\Phi_{\text{sheath}} = 4ZkT_e + 3kT_i$ , and the local angle of incidence is used in the calculation.

The numerical scheme used to produce the entering distributions first randomly selects a poloidal position on the limiter, and then finds the minor radius depth in the SOL ( $\rho_{\text{LCFS-a}}$ ) and the value of the local tile surface tangent at that poloidal location. This is needed to find the angular distribution of velocity cosines. The generation code produces a file of self-consistent values of  $\rho_{\text{LCFS-a}}$ , local tangent and sheath potential ( $\Phi$ ) as a function of poloidal angle. A random number generator then picks the specific location for emission of a new particle from the range of values in this file. The velocity parameters, are similarly obtained. The particles which are emitted may be either  $C^0$  or  $CD_4$ , depending on whether physical or chemical sputtering is under study.

### Particle transport in the SOL

Each particle incident from the limiter is tracked until its final disposition. The particles are assumed to diffuse both parallel and perpendicular to a defined set of magnetic flux surfaces. The parameters used in this description are obtained from Tore Supra magnetics fitting routines. The equation describing the flux surfaces is

$$\rho^2 = (R - R_{\text{plasma}})^2 + (z - z_{\text{shift}})^2/\kappa^2 ,$$

where  $R$  is major radius,  $R_{\text{plasma}}$  is the major radius of the plasma center,  $z$  is the vertical coordinate,  $z_{\text{shift}}$  is the vertical displacement of the plasma,  $\kappa$  is the plasma elongation ( $<1$  in the case of oblateness), and  $\rho$  is the flux surface label.

The particles are flown on straight line tracks until the first ionization, or subsequent to recombination into the neutral state. While charged, the particles are flown on

flux surfaces as described by the magnetics model, and the free streaming along field lines and by random diffusive processes are calculated. The maximum allowable step size is pre-determined (usually set at  $0.01 \times$  the grid resolution), and a track length estimator is used to choose a time step. The track length estimator uses a first ionization probability of 10% to estimate the step length for neutral particles, or 10% of the next stage ionization distance to estimate the step length for charged particles. Subsequent steps are handled differently, depending on whether the particles are charged or not.

For neutral particles, the equations of motion are Cartesian, while for charged particles, the particle motion consists of free streaming parallel to the flux surface defined by the current value of the safety factor ( $q$ ) along with the random diffusion and heating processes. In this case the particle dynamics are described by advancing the variables  $\theta$ ,  $\phi$ , and  $\rho$ , the poloidal and toroidal angles and the flux surface label. The step in toroidal angle ( $\Delta\phi$ ) is chosen using the track length estimator to obtain a value for  $dt$ . Then the toroidal step is determined by using the current value of the toroidal velocity,  $\Delta\phi = v_\phi dt$ .

The equations which then advance the variables are, first the free streaming along the field:

$$\phi_{\text{new}} = \phi + \Delta\phi ,$$

$$\theta_{\text{new}} = \theta + \Delta\phi/q(\psi) .$$

With the parallel diffusivity given by its Spitzer value,

$$D_{\parallel} = (8 EZ/3\pi M_i)\tau_Z(Z,\rho) .$$

a random value  $\xi[-1,1]$  is chosen, and the toroidal and poloidal random diffusion steps are:

$$\Delta\phi_{\parallel} = \xi(D_{\parallel} dt E/R)^{1/2} ,$$

and

$$\Delta\theta_{\parallel} = \Delta\phi_{\parallel}/q(\psi) .$$

Motion due to the background friction force is described by:

$$\Delta\phi_{\text{friction}} = 0.5 dt^2 [v_{\text{background}}(\rho,q) - v]/\tau_s(Z,\rho)/R$$

with

$$\Delta\theta_{\text{friction}} = \Delta\phi_{\text{friction}}/q(\psi) .$$

The model used in BBQ for  $v_{\text{background}}$  assumes a local flux amplification  $A = 2$  near the limiter.

Motion due to the local electrostatic field is described by:

$$\begin{aligned}\Delta\phi_{\text{electrostatic}} &= (1/2)ZeE_{\text{SOL}} dt^2/A/R \\ &= 0.5 dt^2 Z c_{\text{sound}}(\rho) M(\rho, q)/A/R \\ \Delta\phi_{\text{electrostatic}} &= \Delta\phi_{\text{electrostatic}}/q(\psi)\end{aligned}$$

The cross-field diffusion is given by

$$\rho_{\text{new}} = \rho + (1 - 2\xi)(D_{\perp} dt)^{1/2} \text{ with } \xi \text{ random in } [0,1] .$$

The thermal balance for the particles is calculated. It contains contributions due to thermalization with the background ions,

$$E_{\text{new}} = E [1 - dt \tau_h(Z, \rho)] + dt \tau_h(Z, \rho) T_i(\rho)$$

from frictional heating,

$$v_{\text{new}} = v [1 - dt \tau_s(Z, \rho)] + dt \tau_s(Z, \rho) v_{\text{background}}(r, q)$$

and from the electrostatic field,

$$v_{\text{new}} = v dt Z * c_{\text{sound}}(r) * M(\rho)/A/R .$$

New velocity angles are chosen to follow field lines, given the new spatial angles  $\phi_{\text{new}}$  and  $\theta_{\text{new}}$ .

Each particle, whether neutral or charged, is evaluated for the chance of undergoing ionization, and recombination if charged. Upon first ionization we obtain the pitch angles with respect to the field from the requirement that  $\mathbf{v} \cdot \mathbf{B}_{\text{new}} = \mathbf{v} \cdot \mathbf{B}_{\text{old}}$ . Particle flights are terminated when they strike a PFC, or penetrate to within a predetermined depth inside the core plasma. When particles strike a PFC, their positions and the local sheath potential are tallied, and at the end of the run these results output as a file for subsequent runs to assess the contributions due to self-sputtering. The depth inside the last closed flux surface at which particles are terminated is usually 1 cm. Because of the possibility that particles which penetrate inside the last closed flux surface can diffuse into the center of the plasma, thus leading to impractically long execution times, particles are tracked up to a maximum time limit, which is pre-determined. This limit is 15 ms for the cases presented, while the characteristic lifetimes are <1 ms. Fewer than 1% of particles are stopped by this requirement.

## Experimental Setup

An existing endoscope system previously used for infrared (IR) measurements was modified for imaging in the visible range of the spectrum. The modification was designed such that the internal IR optics could be reproducibly replaced by the visible optics, and

vice-versa. In addition, a beam splitter was introduced into this system so that the light could be directed simultaneously to a CCD camera and to a set of optical fibers. This way, the CCD camera provides the high spatial resolution for the entire limiter, while the optical fibers, coupled to a dedicated visible spectrometer, provide the absolute calibration and the spectral resolution. Figure 2 shows a schematic of this system. The CCD camera was equipped with a filter wheel, containing interference filters for the  $D_{\alpha}$  6561 Å, CII 5150 Å, and CIII 4647 Å lines, respectively. By using an asynchronous controller for the CCD camera, the integration time could be varied over a large range (typically 0.2 to 200 ms) to control the effective gain of the camera. The limited dynamic range of the CCD camera required duplicating each plasma shot, so that the image could be optimized for either the bright leading edge or the dimmer front face. The spectrometer was equipped with an Optical Multichannel Analyser (OMA). Exposure times varied between 0.1 and 1.5 s, depending on the plasma conditions and the spectral line observed.

Absolute intensity calibration is an essential requirement for these measurements and is performed whenever access to the interior of the vacuum vessel is possible. The endoscope, optical fibers, and spectrometer are calibrated as a system using a standard source. The calibration is then transferred to the CCD images when analyzing shot data.

## Experimental Results

This campaign included electron density scans in the range of  $1.6$  to  $3.5 \times 10^{19} \text{ m}^{-3}$  (volume averaged) and a plasma current scan in the range of 0.8 to 1.49 MA in  $D_2$  plasmas. For each of these conditions, all at  $B_T = 3.7 \text{ T}$ , sets of similar shots were produced, so that all three lines spectral lines (CII, CIII, and  $H_{\alpha}$ ) could be monitored with the spectrometer and with the CCD camera simultaneously.

In this paper, we present data from the case of  $\langle n_e \rangle = 3.0 \times 10^{19} \text{ m}^{-3}$  and  $I_p = 1.24 \text{ MA}$ . An apparent increase in the emission at the limiter leading edge was observed in the CCD filtered images, as a function of time. This increase was later shown, by means of the spectrometer data (Fig. 3), to be due to increases not in the line intensity, but in the underlying continuum caused by significant heating ( $>1000^{\circ}\text{C}$ ) of the limiter. Thus, interpretation of the data requires a separation of the effects of continuum and line radiation. Here we restrict our analysis to times early enough in the limiter heating phase that the continuum radiation is not yet dominant (i.e., to  $t \leq 6 \text{ s}$  in the discharge, where limiter heating begins at  $t = 4 \text{ s}$ ).

“Grayscale” images of the spatial distributions of  $H_{\alpha}$ , CII and CIII at  $t = \sim 6 \text{ s}$  are shown in Fig. 4 (a,b,c, respectively). Note in the CII image that the maxima in emission occur at the locations where the heat flux and limiter temperature are expected to peak (Fig. 1). Since CII emission is more closely tied to the impurity neutral source than CIII, this may be taken as an indication, independent of modeling, as to the localization of the impurity source. In this case the emission appears to be closely correlated with the expected maxima in limiter temperature distribution, and this gives an indication that chemical sputtering may be involved for this data set.

## Modeling results

Modeling of this data set with the BBQ code has been carried out to compare the predicted CII and CIII distribution with those observed. The code requires the specification of a number of parameters describing SOL transport. For this data set, the following values were used:

$D_{\perp}$	$D_{\parallel}$	$T_e^{\text{lim}}$	$T_i^{\text{lim}}$	$\lambda_q$	$\lambda_{\Gamma}$
1 m <sup>2</sup> /s	50 m <sup>2</sup> /s	35 eV	15 eV	1 cm	2.5 cm

The background plasma parameters are obtained from Langmuir probe data and the flux surfaces from magnetics. The code predicts the spatial distribution of  $C^{n+}(\rho, \phi, \theta)$  from an assumed source of combined chemical and physical sputtering. The ratio of ionization to photon events ( $S/XB$ ) is taken from [12] to generate a distribution of CII and CIII emission. The result is a predicted distribution of impurity light. In Fig. 5 we compare the distributions of CII light for the case of Fig. 4(b) assuming (a) only a physical sputtering source and (b) a combined physical and chemical sputtering source. Qualitatively, the occurrence of a sharp peak at the limiter leading edge and also on the limiter crown requires a chemical sputtering source. An total ion flux of 50 A (or 50 torr l/s) and a 70:30 ion to electron drift-side asymmetry were assumed for these modeling runs.

## DISCUSSION AND CONCLUSIONS

We have examined the spatial distribution of impurity sources on the front face of the Phase I outboard limiter for the simple case of a small plasma, which is only in contact with this limiter. Using the BBQ code, we can successfully model the measurements when we include chemical sputtering in the impurity generation processes. The estimated surface temperatures ( $T_{\text{surf}}$ ) of the limiter, from IR camera images taken during similar shots, were in the range 625 to 795°C on the leading edge and about 600°C on the front face. In such a temperature range, chemical sputtering is expected to be significant (see Roth et al. in [5]). Although, in the literature, chemical sputtering data are limited to ion fluxes several orders of magnitude lower than those encountered in a tokamak limiter, previous results on the Phase II pump limiter showed this process to be important near the neutralizer plate [3]. There, the ion flux was measured to be about  $2 \times 10^{19}$  ions/cm<sup>2</sup>/s.

The oxygen content is normally negligible in Tore Supra, especially since boronization became a standard procedure. It is therefore assumed that oxygen plays no role in the sputtering process. The strong dependence of the chemical sputtering process on  $T_{\text{surf}}$  [5] is primarily responsible for the large difference between the two modeling results in Fig. 5. The expected large difference in the energies and ionization path lengths of molecules created by chemical sputtering to mostly atomic C generated by the physical sputtering mechanism also plays a large role.

## Future work

An immediate next step will be to examine the measured impurity distributions at later times ( $t > 6$  s) in these discharges to determine the importance of the various sputtering processes as  $T_{\text{surf}}$  increases (e.g., the possible role of RES or thermionic emission). When a new series of experimental runs begins with the newly installed Phase III pump limiter, we plan to repeat these measurements and compare results with those of the inertial limiter. In the new measurements, we will include a spectral survey to search for molecular bands, whose existence is implied by our assumption that chemical sputtering plays a role in the impurity production.

Ultimately, the goal of the multilimiter setup in Tore Supra is to optimize power sharing between all the PFCs without sacrificing plasma performance and particle removal capabilities [13], [14]. In parallel with this program we plan to study the impurity generation processes from the lower pump limiters and antennas and examine the synergy in these processes arising from the connection (by means of magnetic field lines) between these PFCs. In the case of the radio frequency (rf) antenna, some observations of CIII profiles have already been carried out in an initial study to evaluate damage to the antenna shields due to rf-induced potentials [15].

## ACKNOWLEDGMENTS

The authors wish to acknowledge the valuable advice from C. E. Thomas and J. H. Harris of ORNL on the analysis of the CCD camera images and to thank P. K. Mioduszewski of ORNL for his support and encouragement throughout this project. The efforts of M. Chatelier and C. DeMichelis of CEA-Euratom in organizing this project at Tore Supra are also acknowledged.

## REFERENCES

- [1] A. Seigneur, D. Guilhem, J. T. Hogan, et al., *Proc. of the 20th EPS Conf. on Contr. Fusion and Plasma Phys.*, Lisbon (26–30 July 1993), II-603.
- [2] C. C. Klepper, J. T. Hogan, et al., “Characterization of Atomic and Molecular Impurity Sources and Transport at the Tokamak Edge” in *Atomic Processes in Plasmas*, AIP Conference Proceedings (San Antonio, 1993), W. L. Rowan, Editor.
- [3] C. C. Klepper, J. T. Hogan, and L. W. Owen, et al., *Proc. of the 20th EPS Conf. on Contr. Fusion and Plasma Phys.*, Lisbon (26–30 July 1993), II-599.
- [4] P. C. Stangeby, *J. Nucl. Mater.* **176&177** (1990), 51–64.
- [5] Atomic and Plasma-Material Interaction Data for Fusion (supplement to *Nuclear Fusion*), 63–78 (1991).
- [6] W. D. Langer and A. B. Ehrhardt, *J. Nucl. Mater.* **162–164** (1989), 329–336.
- [7] J. T. Hogan and A. Pospieszczyk, “Modeling of hydrocarbon fueling” ORNL Report, ORNL/TM-11542, July 1990.

- [8] R. Nygren et al., "Steady State Heat and Particle Removal with the Actively Cooled Phase III Outboard Pump Limiter in Tore Supra" (to be published in PSI '94 Conference Proceedings).
- [9] C. C. Klepper, T. Uckan, P. K. Mioduszewski, R. T. McGrath, and P. Hertout, *Fusion Technology*, Vol. 14, No. 2 (Sept. 1988), pp. 288–298.
- [10] J. B. Whitley et al., *Proc. 14th Symp. Fusion Technology*, Avignon, France (Sept. 8–12, 1986), pp. 627, Pergamon Press.
- [11] J. A. Koski et al., *Proc. ANS (Session on Fundamental of Fusion Reactors, Thermal Hydraulics)*, San Francisco, 1991
- [12] K. Behringer, H. P. Summers, B. Denne, M. Forrest, and M. Stamp, *Plasma Phys. Contr. Fusion* **31**, 2059 (1989)
- [13] R. T. McGrath., C. C. Klepper, T. Uckan, and P. K. Mioduszewski, *Fusion Technology*, Vol. 14, No. 2 (Sept. 1988), pp. 339–353.
- [14] T. Uckan, C. C. Klepper, P. K. Mioduszewski, R. T. McGrath, *Fusion Technology*, Vol. 13, No. 1 (Jan. 1988), pp. 165–180.
- [15] C. E. Thomas, Jr. et al., "First Results from Experimental Measurements of ICRF and Edge/SOL Plasma Interactions on Tore Supra" (to be published in PSI '94 Conference Proceedings).

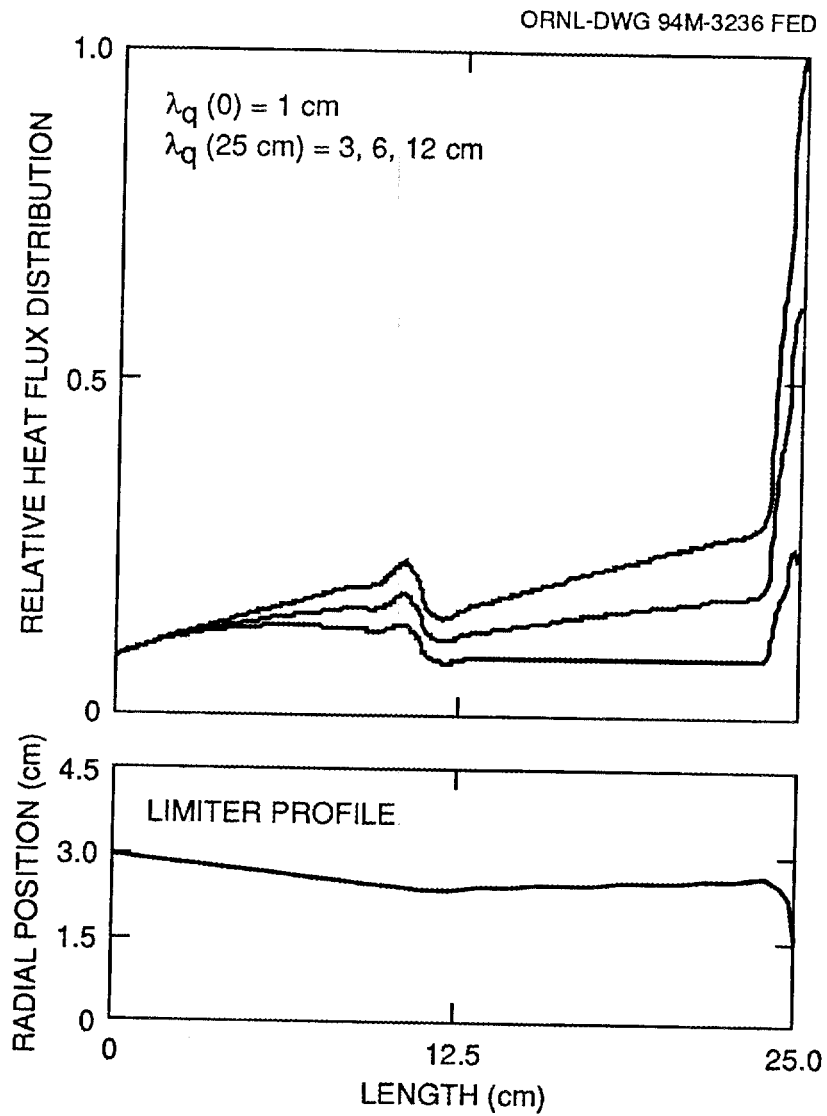


Fig. 1. Shape of the toroidal cross-section of the limiter and predicted heat flux distribution for the design case of  $R = 2.38 \text{ m}$ ,  $a = 0.75 \text{ m}$  for various values of the heat flux decay length ( $\lambda_q$ ) [11].

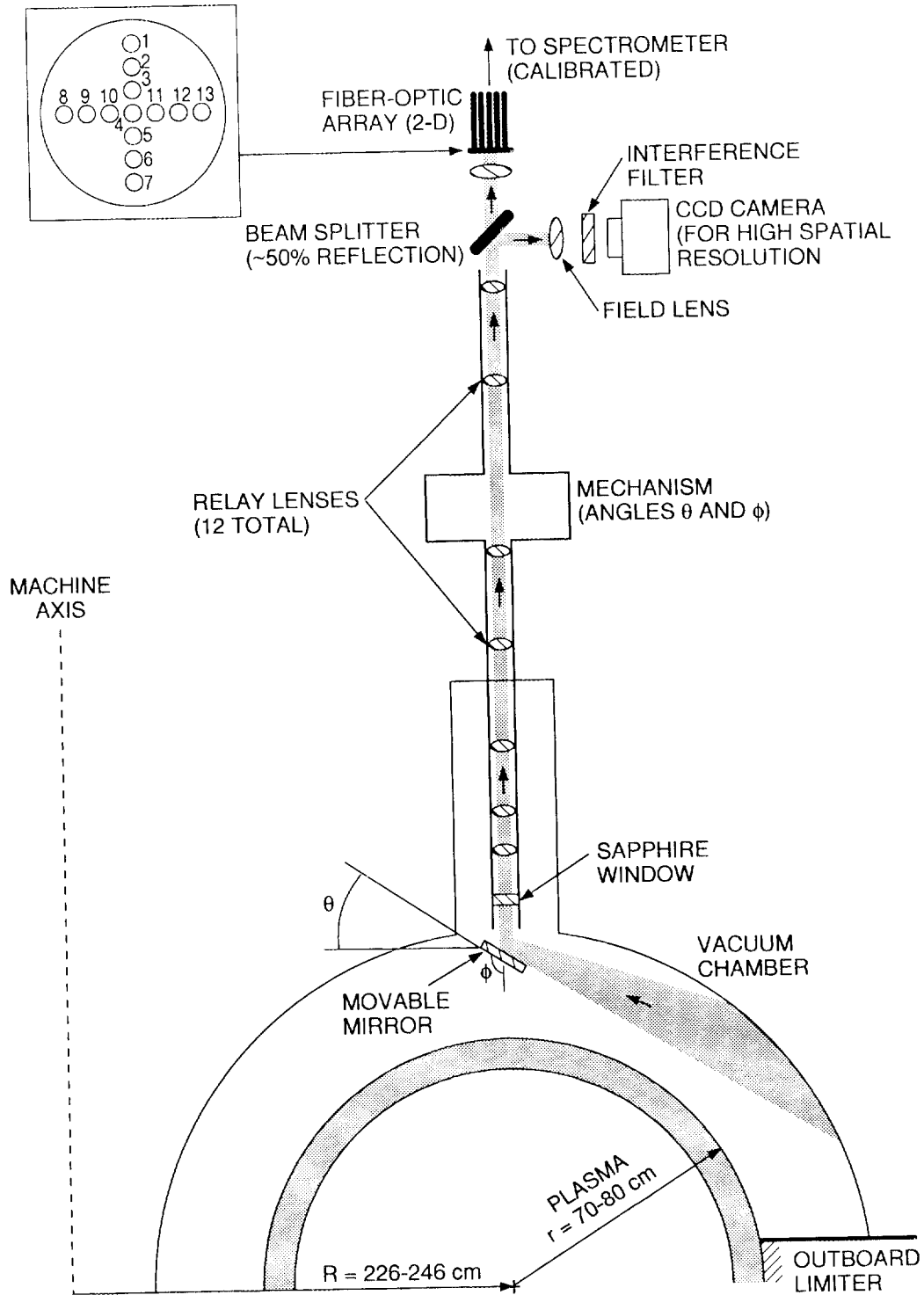


Fig. 2. Schematic of the endoscopic optical imaging system, which permits simultaneous 2-D spatial imaging and calibrated spectra.

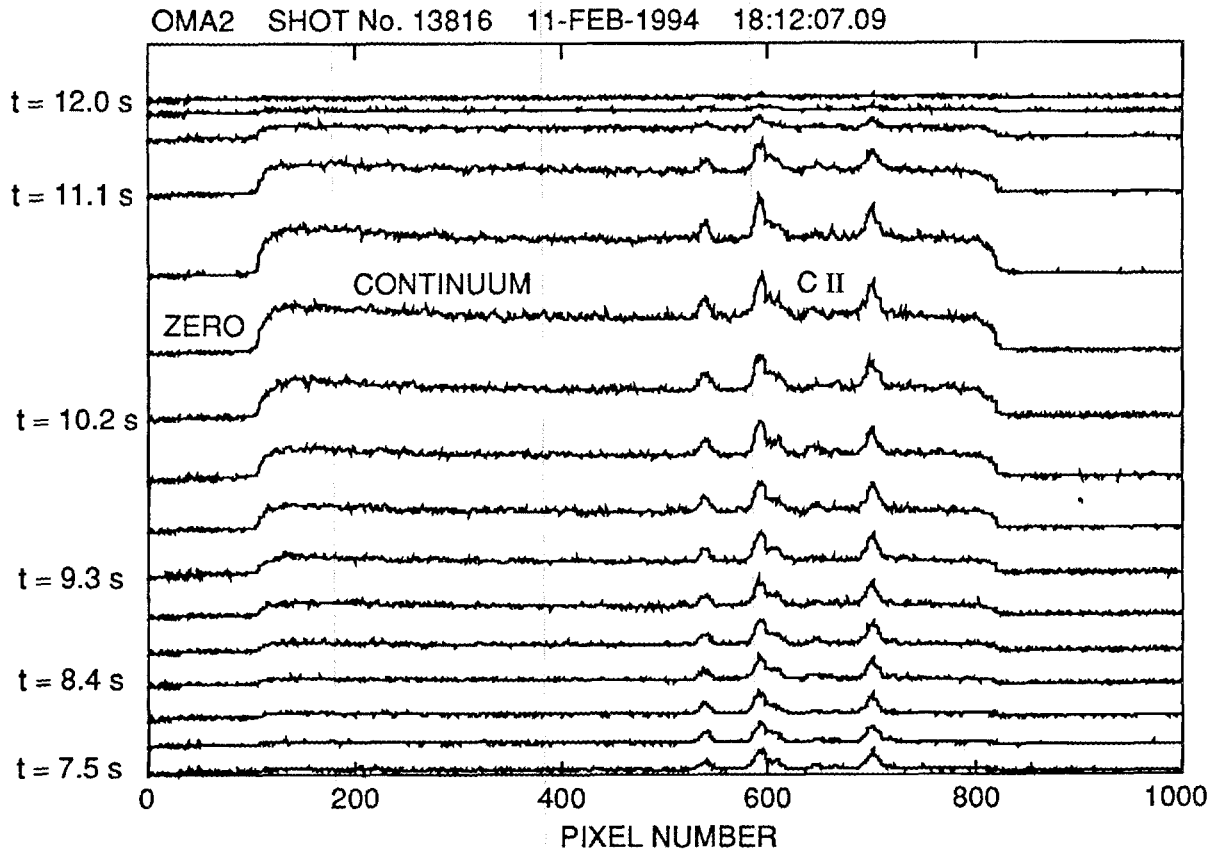


Fig. 3. Evolution in time of the spectrum containing a set of CII lines near  $5140 \text{ \AA}$ , showing the increase in the continuum due to the blackbody radiation. The zero reference level on both sides of the spectrum is a result of the size of the intensifier, which is smaller than the photodiode array of the OMA.

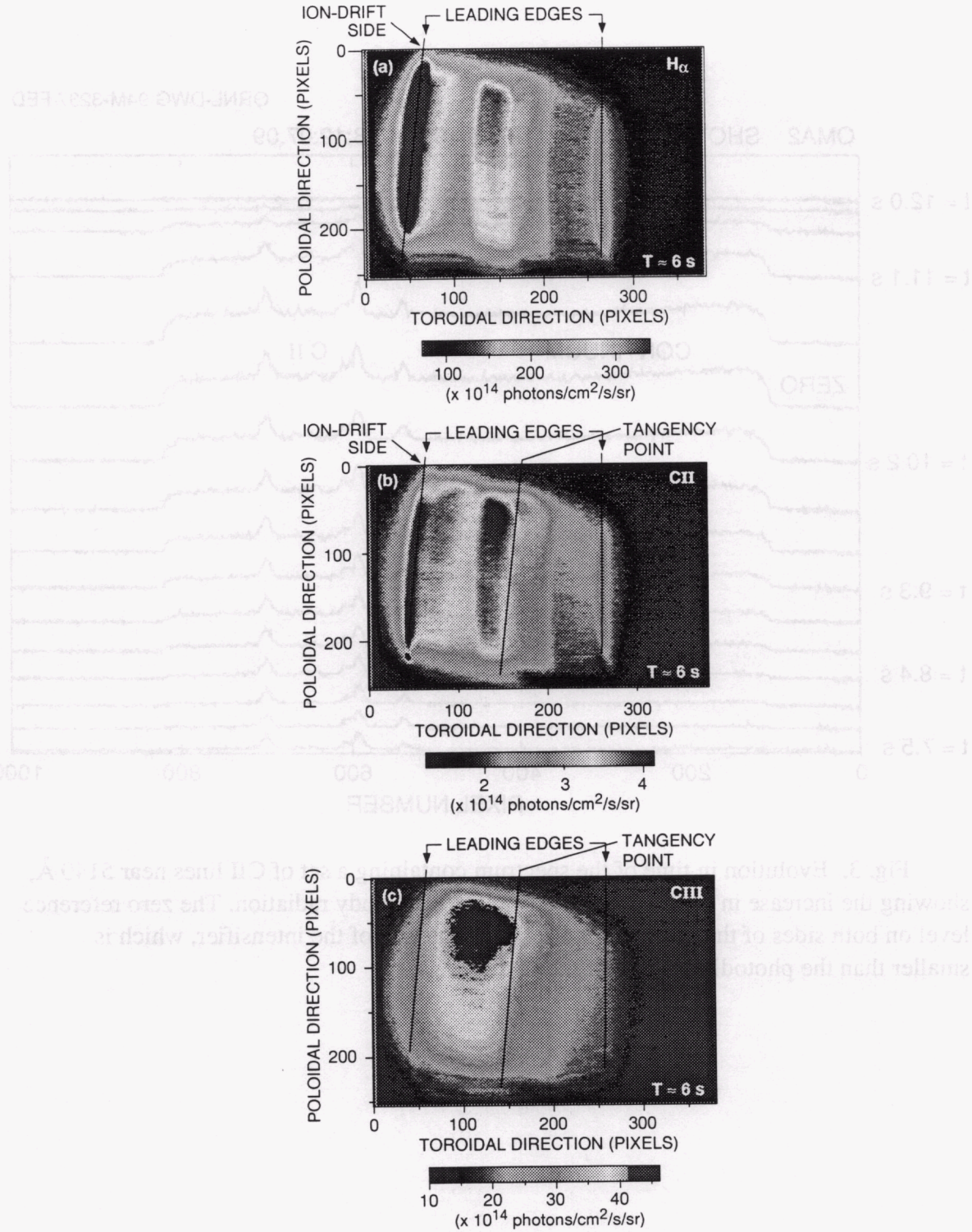


Fig. 4. "Grayscale" images of the measured spatial distributions of (a)  $H_{\alpha}$ , (b) CII, and (c) CIII at  $t = -6$  s.

ORNL-DWG 94M-3239 FED

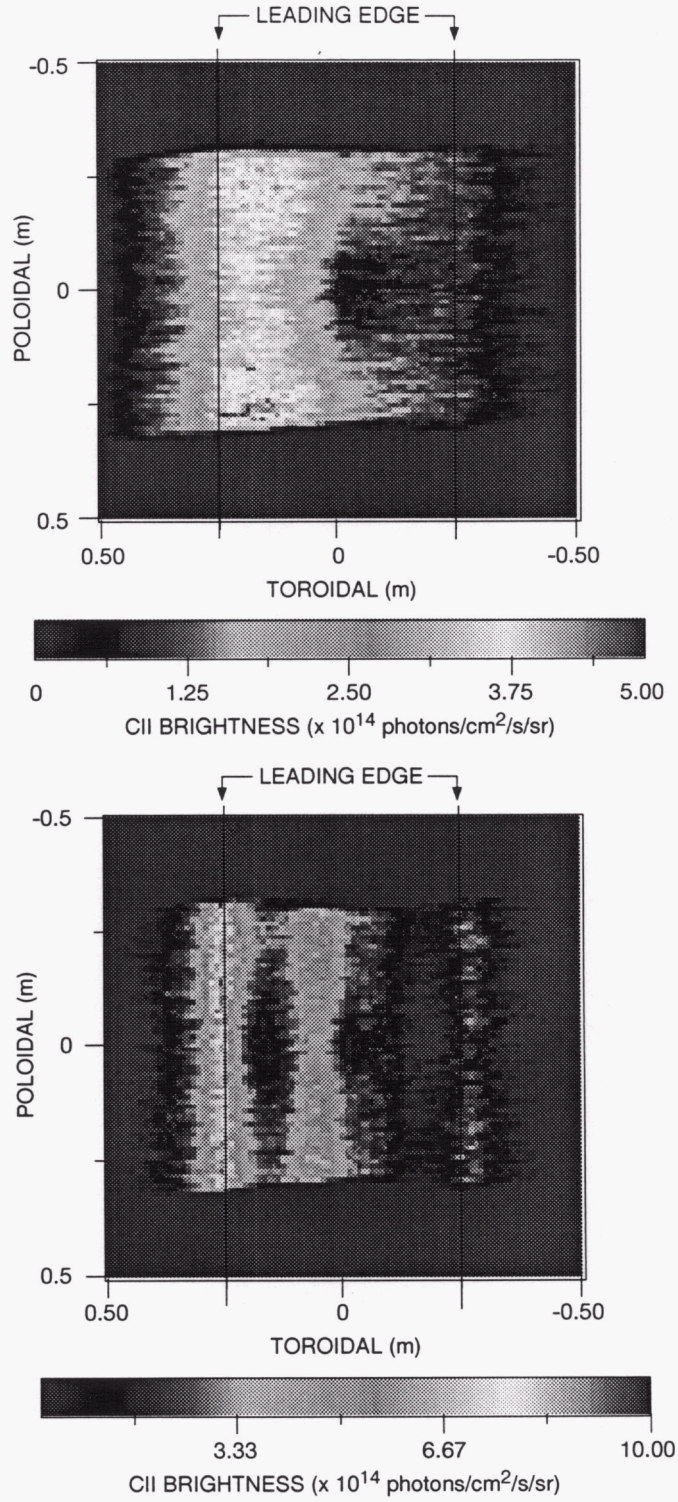


Fig. 5. "Grayscale" images of the predicted (with BBQ) spatial distributions of CII assuming (a) only physical sputtering and (b) both physical and chemical sputtering.



**INTERNAL DISTRIBUTION**

- |   |   |
|---|---|
| 1. Director, ORNL Fusion Energy<br>Division | 11. R. P. Leinius   |
| 2. C. C. Baker                              | 12-13. Laboratory Records<br>Department                                     |
| 3. L. A. Berry                              | 14. Laboratory Records, ORNL-RC   |
| 4. B. A. Carreras                           | 15-16. Central Research Library   |
| 5. R. A. Dory                               | 17. Document Reference Section  |
| 6. D. J. Hoffman                            | 18. Fusion Energy Division Library  |
| 7. J. F. Lyon                               | 19-20. Engineering Technology/Fusion<br>Energy Division Publications Office |
| 8. M. S. Lubell                             | 21. ORNL Patent Office  |
| 9. S. L. Milora                             | 22-26. C. C. Klepper  |
| 10. T. E. Shannon                           |   |

**EXTERNAL DISTRIBUTION**

27. Office of the Assistant Manager for Energy Research and Development, U.S. Department of Energy Oak Ridge Operations, P.O. Box 2000, Oak Ridge, TN 37831
28. N. A. Davies, Director, Office of Fusion Energy, Office of Energy Research, ER-50 Germantown, U.S. Department of Energy, Washington, DC 20545
29. M. Roberts, International Programs, Office of Fusion Energy, Office of Energy Research, ER-52 Germantown, U.S. Department of Energy, Washington, DC 20545
30. D. E. Baldwin, Lawrence Livermore National Laboratory, P.O. Box 5511, Livermore, CA 94550
31. R. W. Conn, Mechanical, Aerospace, and Nuclear Engineering Department, 6291 Boelter Hall, University of California, Los Angeles, CA 90024-1597
32. P. C. Liewer, MS 138-208, Jet Propulsion Laboratory, 4800 Oak Grove Drive, Pasadena, CA 91109
33. R. Parker, Plasma Fusion Center, Massachusetts Institute of Technology, 167 Albany St., NW16-288, Cambridge, MA 02139
34. K. I. Thomassen, L-637, Lawrence Livermore National Laboratory, P.O. Box 5511, Livermore, CA 94550
35. J. D. Callen, Department of Nuclear Engineering, University of Wisconsin, Madison, WI 53706-1687
36. S. O. Dean, Fusion Power Associates, Inc., 2 Professional Drive, Suite 248, Gaithersburg, MD 20879
37. H. K. Forsen, Bechtel Group, Inc., Research Engineering, P.O. Box 3965, San Francisco, CA 94119
38. R. W. Gould, Department of Applied Physics, California Institute of Technology, Pasadena, CA 91125
39. R. A. Gross, Plasma Research Laboratory, Columbia University, New York, NY 10027

40. R. J. Hawryluk, Princeton Plasma Physics Laboratory, P.O. Box 451, Princeton, NJ 08543
41. D. M. Meade, Princeton Plasma Physics Laboratory, P.O. Box 451, Princeton, NJ 08543
42. W. M. Stacey, School of Nuclear Engineering and Health Physics, Georgia Institute of Technology, Atlanta, GA 30332
43. D. Steiner, Nuclear Engineering Department, NES Building, Tibbetts Avenue, Rensselaer Polytechnic Institute, Troy, NY 12181
44. R. Varma, Physical Research Laboratory, Navrangpura, Ahmedabad 380009, India
45. Bibliothek, Max-Planck Institut für Plasmaphysik, Boltzmannstrasse 2, D-8046 Garching, Federal Republic of Germany
46. Bibliothek, Institut für Plasmaphysik, KFA Jülich GmbH, Postfach 1913, D-5170 Jülich, Federal Republic of Germany
47. Bibliothek, KfK Karlsruhe GmbH, Postfach 3640, D-7500 Karlsruhe 1, Federal Republic of Germany
48. Bibliotheque, Centre de Recherches en Physique des Plasmas, Ecole Polytechnique Fédérale de Lausanne, 21 Avenue des Bains, CH-1007 Lausanne, Switzerland
49. D. Escande, CEN/Cadarache, Departement de Recherches sur la Fusion Contrôlée, F-13108 Saint-Paul-lez-Durance Cedex, France
50. R. Aymar, Director ITER-EDA, San Diego, 11025 N. Torrey Pines Road, La Jolla, CA 92037
51. Bibliothèque, CEN/Cadarache, F-13108 Saint-Paul-lez-Durance Cedex, France
52. Library, JET Joint Undertaking, Abingdon, Oxfordshire OX14 3EA, England
53. Library, FOM-Instituut voor Plasmafysica, Rijnhuizen, Edisonbaan 14, 3439 MN Nieuwegein, The Netherlands
54. Library, National Institute for Fusion Science, Chikusa-ku, Nagoya 464-01, Japan
55. Library, International Centre for Theoretical Physics, P.O. Box 586, I-34100 Trieste, Italy
56. Library, Centro Ricerca Energia Frascati, C.P. 65, I-00044 Frascati (Roma), Italy
57. Library, Plasma Physics Laboratory, Kyoto University, Gokasho, Uji, Kyoto 611, Japan
58. Plasma Research Laboratory, Australian National University, P.O. Box 4, Canberra, A.C.T. 2601, Australia
59. Library, Japan Atomic Energy Research Institute, Naka Fusion Research Establishment, 801-1 Mukoyama, Naka-machi, Naka-gun, Ibaraki-ken, Japan
60. G. A. Eliseev, I. V. Kurchatov Institute of Atomic Energy, P.O. Box 3402, 123182 Moscow, Russia
61. V. A. Glukhikh, Scientific-Research Institute of Electro-Physical Apparatus, 188631 St. Petersburg, Russia
62. I. Shpigel, Institute of General Physics, Russia Academy of Sciences, Ulitsa Vavilova 38, Moscow, Russia
63. D. D. Ryutov, Institute of Nuclear Physics, Sovetskaya St. 5, 630090 Novosibirsk, Russia
64. O. Pavlichenko, Kharkov Physical-Technical Institute, Academical St. 1, 310108 Kharkov, Ukraine

65. Deputy Director, Southwestern Institute of Physics, P.O. Box 15, Leshan, Sichuan, China (PRC)
66. Director, The Institute of Plasma Physics, P.O. Box 1126, Hefei, Anhui, China (PRC)
- 67-104. Given distribution as shown in DOE/OSTI-4500-R75, under category UC-420, Magnetic Fusion Energy